Battery Current and Temperature Mission Profiles for CubeSats at Low Earth Orbit

Knap, Vaclav; Beczkowski, Szymon Michal; Vestergaard, Lars Kjeldgaard; Stroe, Daniel-Ioan

Published in:
I E E E Transactions on Aerospace and Electronic Systems

DOI (link to publication from Publisher):
10.1109/TAES.2022.3164867

Publication date:
2022

Document Version
Accepted author manuscript, peer reviewed version

Battery Current and Temperature Mission Profiles for CubeSats at Low Earth Orbit

Vaclav Knap, Szymon Beczkowski, Lars Kjeldgaard Vestergaard, Daniel-Ioan Stroe, *Member, IEEE*

***Abstract*—CubeSats, a branch of the space industry, has lately received great interest for being an affordable satellite platform. For proper functioning, they are nowadays practically dependent on Lithium-ion batteries as a power supply at moments, when there is not enough power generated by solar panels. Thus, batteries have to be thoroughly tested to ensure that they provide sufficient performance, lifetime and that they are safe. In other industry areas, such as electric vehicles, it is common to use mission profiles (often referred to as driving profiles) for battery testing to closely emulate conditions that are experienced in practice. However, mission profiles reflecting closely CubeSat conditions are not publicly available. Thus, this paper proposes a methodology to derive mission profiles, and resulting representative mission profiles, dedicated especially to battery testing. The proposed methodology is based on analyzed telemetry data from three GOMX CubeSats. At first, electrical current characteristics are obtained from the telemetry and are generalized across the satellites, to be subsequently used for the mission profile synthesis. The battery temperature is an important factor for the battery performance and lifetime, and it was identified to be very dynamic in CubeSats. Thus, a model describing battery temperature during their mission is proposed to enable generate realistic temperature mission profiles. Finally, the current and temperature profiles are synchronized to capture their mutual impact on the batteries, and they are formulated to be suitable for on-ground (laboratory) testing.**

***Index Terms*—cubesat, lithium-ion battery, low earth orbit, mission profile, nano-satellite, testing.**

NOMENCLATURE

Abbreviations and acronyms

ADS-B	Automatic-dependent surveillance-broadcast
AIS	Automatic identification system
BTS	Battery test station
CC	Constant current
CC-CV	Constant current - constant voltage
COTS	Commercial-off-the-shelf
DOD	Depth of discharge
ESA	European Space Agency
HF	High frequency
IOD	In-orbit demonstration
LEO	Low Earth orbit
LF	Low frequency
NASA	National Aeronautics and Space Administration
RMSE	Root-mean-square-error
SMP	Synthetic mission profile
SOC	State-of-charge
SSO	Sun synchronous orbit

Variables

$\square_{\mathrm{x}}$	Subscript x used to distinguish current directions: c for charging and d for discharging
$\mathbf{I}_{\mathrm{x,h,i}}$	Current vector determined via histograms for i-th satellite
$\mathbf{R}_{\mathrm{x,h,i}}$	Current occurrence ratio vector determined via histograms for i-th satellite
$\langle \mathbf{I}_{\mathbf{x,h}} \rangle_{\mathrm{sat}}$	Aggregated current vector determined via histograms across satellites
$\langle \mathbf{R}_{\mathbf{x,h}} \rangle_{\mathrm{sat}}$	Aggregated current ratio vector determined via histograms across satellites
$\langle I_{\mathrm{x,h}} \rangle_{\mathrm{sat,orbit}}$	Average current in an orbit across satellites
$\langle \mathbf{I}_{\mathbf{x,n}} \rangle_{\mathrm{sat}}$	Normalized aggregated current vector
n	Number of satellites
τ_{orbit}	Orbit time duration
E_{r}	Eclipse duration as a fraction of an orbit
L_{r}	Lag in charging
$\hat{\tau}_{\mathrm{x}}$	(Dis)charging time
k_{AF}	Test accelerating factor by which is an orbit duration shortened
C_{dod}	Capacity depth-of-discharge that is charged and discharged during one orbit
$\langle \hat{I}_{\mathrm{x}} \rangle_{\mathrm{orbit}}$	Average (dis)charging current during orbit
$\hat{\mathbf{I}}_{\mathrm{x}}$	Vector of current values for a specific mission profile
$\eta_{\mathrm{I,x}}$	Coulombic efficiency of battery cells, battery packs, and/or electrical power supply
β_S	Angle between the orbital plane of the satellite and the vector to the Sun
a, b, c, d	Parameters of the temperature model
t	Time
$\tau_{\beta_{\mathrm{S}}}$	Low frequency period
$\phi_{\beta_{\mathrm{S}}}$	Low frequency phase shift
ϕ_{orbit}	High frequency phase shift

This work was supported by Innovation Fund Denmark (Grant No: 8054-00027B).

V. Knap and L.K. Vestergaard are with GomSpace A/S, Denmark (e-mail: vakn@gomspace.com; lav@gomspace.com).

V. Knap is with Faculty of Electrical Engineering, Czech Technical University in Prague, Czech Republic (e-mail: knapvacl@fel.cvut.cz).

V. Knap, S. Beczkowski, and D.-I. Stroe are with Department of Energy Technology, Aalborg University, Denmark (e-mail: vkn@et.aau.dk; sbe@et.aau.dk; dis@et.aau.dk).

I. INTRODUCTION

CUBESATS are a quickly developing area of the space industry [1]. They are generally small sized satellites (1–10 kg nano-, 10–100 kg micro-satellites), with a specific form factor of being composed from 10 cm x 10 cm x 10

cm cubes (1 unit cube = 1U). They can provide a variety of 'classical' satellite services, as well as novel applications, such as internet of things, blockchains, and more. Their most significant benefit is their low manufacturing and launching cost. CubeSats are generally based on commercial-off-the-shelf (COTS) components and they weight in the range of units or tens of kilograms [2].

They are typically equipped with solar panels that cover load consumption and charge batteries during a sunlight, and those batteries then supply the consumption during eclipse periods. The batteries and related technologies are required to be tested to proof their functionality, verify their reliability, and to determine their expected lifetime. The most common approach for on-ground testing, especially to determine battery cycle life, is to cycle them by CC discharging and CC-CV charging modes. The cycling is done in real-time, when a cycle lasts about 90 minutes, i.e., 30 minutes for discharging and 60 minutes for charging, or in accelerated manner, when the time periods are shortened. To emulate LEO conditions, the typical depth of discharge is 10–40% of the nominal capacity [3]–[8]. However, this testing simplification might be different from the real use and some phenomenon might not be triggered/considered. Specifically, it is a case of an impact of different current amplitudes and dynamics on lifetime [9]–[11]. To closer emulate the specific LEO satellite conditions, an arbitrary discharging profile was used for 8s3p battery pack by Giuliani and Remy [12]. They used a discharging profile that was based on a specific mission, which was composed of two constant power discharge periods: 650 W for 30 minutes, and 950 W for 3 minutes, with a combination of CC charge, and the cycle duration of 115 minutes. Alternatively, a constant power discharge and a 'sinusoidal' charge was used to reflect solar panels and irradiance dynamics [13]. From the temperature perspective, the tests are performed at room temperature, or in a thermal chamber at a constant temperature level, relevant to the mission [14]. Besides battery cycle life, it is important to validate also other battery related functionalities, such as state estimation algorithms. A remaining useful life prediction algorithm dedicated to satellites in LEO was developed and applied on battery data set from NASA [15]; however, the battery cycling was again limited only to CC discharging and CC-CV charging operation at deep DOD [16], which oversimplifies the working conditions, and it does not expose the algorithm to the realistic conditions. Subsequently, specific mission profiles were used for validation of state-of-charge (SOC) and state-of-health estimation algorithms [17], [18]. Moreover, a specific flight planner for determining the load together with a simulated solar power generation was used to generate the battery profile and to evaluate the nanosatellite energy control algorithm [19]. In these cases, the algorithms were tested on similar profiles to the ones that they will experience during the mission. However, they are very specific for the considered spacecraft and missions, and they do not support generalization. Thus, a generalized testing profile, or a methodology to derive it for batteries in LEO satellites that would realistically capture the battery operation is missing.

Considering the specifications of a CubeSat application at LEO, an electrical mission profile itself is not enough to closely represent a realistic battery use [20]. CubeSats have a small thermal mass, in contrast to large satellites, and their temperature is strongly influenced by the environment. Thus, the batteries experience significant temperature changes during an orbit. Since the Li-ion batteries are a complex electrochemical system with many processes highly dependent on temperature, the thermal mission profile has to be considered. Typically, the battery performance is reduced at low temperature, as there is a low ionic conductivity caused by increased viscosity of the electrolyte. Other processes, as charge transfer and diffusion are also affected and become sluggish. These changes result then into decreased both power capability and discharging capacity [21]. Moreover, in such conditions the Li-ion batteries are more prone to a lithium plating, which occurs during charging with high current, when potential over the anode becomes negative. Lithium plating causes a rapid degradation, as it consumes lithium ions and it can lead to an internal short circuit, when deposited dendrites penetrate the separator [22]. At high temperatures, the power capability and available discharging capacity are not limited due to the resistance being decreased and the particle transportation being accelerated. However, other parasitic reactions are hastened as well, as for example decomposition of organic components in the solid electrolyte interphase [23], a binder, or lithium salts in the electrolyte [21]. Thus, pronounced self-discharge and degradation occur. Furthermore, when temperature increases even more, it triggers exothermic reactions, which generate excess heat, often leading to a thermal runaway. Consequently, it is important to couple the electrical and the thermal mission profiles in order to capture interactions and possible interplay of various battery characteristics, such as current, voltage, SOC, or temperature.

The need of battery testing at realistic conditions for CubeSats is addressed in this manuscript, which is built upon our previous work presented in [24]. The contributions are stated as:

- a model describing battery temperature in CubeSats during their mission is formulated
- a methodology to derive representative electrical and temperature battery mission profiles from satellite telemetry is proposed
- synchronized and representative current and temperature mission profiles that are suitable for on-ground (laboratory) testing are introduced

In the manuscript, at first, CubeSat missions and their characteristics is introduced in section II, together with the specific missions and spacecrafts used in this work. An overview of the methodology is provided in section III. Afterward, a telemetry analysis and a mission profiles synthesis is performed in section IV, and it is split into three subsections. The first is focused on electrical current domain. The second subsection derives the temperature model. A synchronization of the current and the temperature profiles is described in the third subsection. The experimental section V demonstrates the application of the derived SMPs in the laboratory, and practicalities are discussed. The conclusions and future work are summarized in the last section VI.

II. CubeSats missions

The battery use is driven by a payload and a satellite operation, which is determined by a satellite mission. Thus, the mission overview is provided at first to show that not a single profile can cover in general all the CubeSat missions. Then, the representative examples are selected, and the proposed methodology is applied to them.

A. CubeSat mission overview

CubeSats can conduct different type of missions. Currently, most of them, especially non-scientific ones, are limited to LEO. According to the mission type, the satellite payload, i.e., an equipment directly linked to mission objectives, differ and by that also their power profile and consumption. While the proposed methodology is suitable for any mission and satellite at LEO, the developed SMP is representative only to a specific mission type, according to similarity of its payload. A suitable mission categorization was presented in a report by SpaceWorks [1], which groups them into: Earth observation/remote sensing, communication, science, technology and novel applications.

Earth observation/remote sensing covers areas of various imaging techniques, environmental monitoring (including disasters) and weather monitoring [25]. Specific examples can be found in FACSAT 1 [26], using a camera for urban development, detecting natural disasters, including fires, or illegal land use activities, and Raincube [27], equipped with a precipitation profiling instruments for weather monitoring. Furthermore, tracking of ships (automatic identification system (AIS)) and aircraft (automatic-dependent surveillance-broadcast (ADS-B)) can be considered as remote sensing activities. AIS tracking is performed for example by a Norwegian constellation of AISSat-1,2 and NorSat-1,2 [28]. Historically, nearly 50% of nano/micro-satellites were dedicated to earth observation/remote sensing [1].

Communication missions cover various form of telecommunications, including well established concepts of telephone, television, radio and internet, and as well more modern concepts as internet of things and machine-to-machine data exchange. Large portion of these services is already provided by a constellation '3 Diamonds' [29], [30].

Science missions have no one specific form. They target both Earth orbit and deep space [2], [31]. They focus on study and measurements of Earth, space environment and/or celestial objects [2], [32]. Their focus can partially overlap with technology missions. Since their goals are usually unique, their mission profiles highly depends on considered use and payload, which is often not widely standardized as in the cases of Earth observation/remote sensing and communication.

Technology missions, often referred as In-Orbit-Demonstration (IOD), target to test and proof technological concepts. They represent often a preliminary step for a wide deployment of the previous mission types.

Novel applications or miscellaneous applications cover, what do not fit into other categories. This can include artistic or culture use, as for example demonstrated by project ENOCH [33].

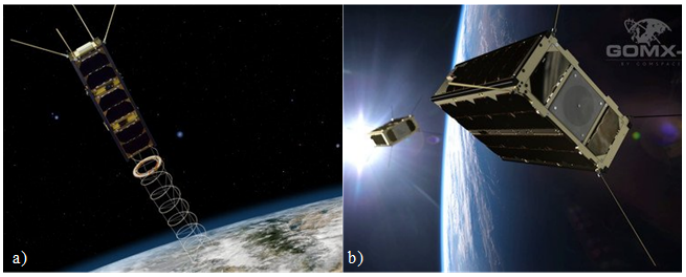

Fig. 1. Illustration of a) GOMX-3 and b) GOMX-4A/B nano-satellites (source: gomspace.com).

B. Representative mission examples

GOMX-3 and GOMX-4A/B satellites, shown in Fig. 1 are used in this work as specific study cases. Their missions served as **technology** demonstrations of mainly **Earth observation/remote sensing**, specifically aircraft and ship tracking.

GOMX-3 was a 3U nano-satellite with missions of technology IOD such as attitude control, high-speed data downlink, radio frequency sensing, and aircraft monitoring ADS-B, for detail description please see [34], [35]. GOMX-3 was launched in October 2015 and it was in operation for about a year, before it re-entered the Earth's atmosphere, in October 2016. It's orbit started at approximately 400 km altitude with inclination of 51.6° (international space station (ISS) orbit).

GOMX-4 mission consists of two 6U satellites GOMX-4A and GOMX4-B, launched in February 2018. The task of GOMX-4A is Arctic surveillance, while GOMX-4B's objective is station keeping capabilities. Together, they prove a concept of inter-satellite linking and aircraft (ADS-B) and ships (AIS) monitoring. For greater detail please see [36], [37]. Both satellites are (until the date of submission) still in operation, performing the tracking activities and occasionally various experiments. Their orbit is sun synchronous orbit (SSO) with inclination around 97.3°, starting at approximately 500 km altitude.

III. Methodology

A typical, simplified structure of a satellite's power system is illustrated in Fig. 2. The scope of this study is limited to batteries and their telemetry. The battery telemetry consists normally of current, voltage, and temperature measurements.

The current can be considered as a control variable, its amplitude controls the battery power output. Consequently, the battery voltage can be considered as a dependent variable on the input current, the battery temperature and the battery inner states (e.g. SOC, polarization voltage). Thus, the telemetry current profile is analyzed and the current mission profile is derived in section IV-A.

Since the batteries experience dynamic temperature swings, mainly due to the small thermal mass of CubeSats, and characteristics of their orbits, the temperature is the second quantity, which is analyzed and its mission profile derived via modelling in section IV-B.

Moreover, it is important for current and temperature mission profiles to be coupled and synchronized. The synchroniza-

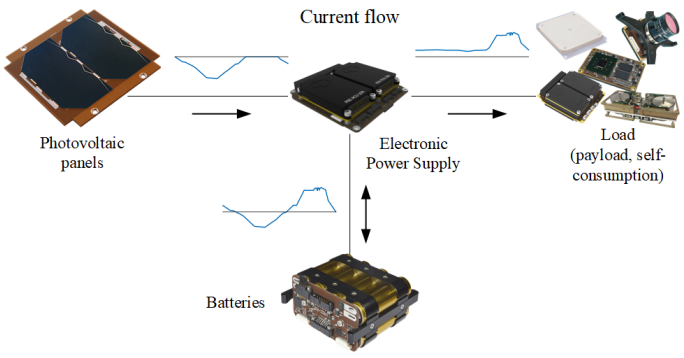

Fig. 2. A simplified illustration of current flow between satellite's generation, consumption and storage.

tion procedure is done via identifying characteristics points (i.e. beginning of charging) and it is presented in section IV-C.

The overview of the whole procedure is illustrated in Fig. 3. At first, the telemetry is processed to extract relevant representative characteristics. Afterward, the mission profiles are synthesized by specifying orbit and battery testing parameters.

The specific battery telemetry is obtained from GOMX-3 and GOMX-4A/B CubeSats. GOMX-3 was equipped with a battery pack BP4, consisting of 4 cells in configuration 4s-1p [38]. GOMX-4A/B are equipped with battery packs BPX with 8 cells in configuration 4s-2p [39]. The telemetry data are scaled down to a single battery cell. The battery cells used for the CubeSat battery packs are 2.6 Ah Li-ion cells [40].

IV. Telemetry Analysis and Mission Profile Synthesis

A. Current

The current telemetry was obtained from the satellites in the following periods: October 2015 to October 2016 for GOMX-3, February 2018 to February 2020 for GOMX-4A and GOMX-4B. The battery pack current was recomputed to a battery cell current and it is shown in Fig. 4.

1) Current telemetry analysis: One way to assess the current data is through histograms, for which the current was separated into charging (negative) and discharging (positive). When histograms are applied to the data collected over a long period, they express an occurrence of current amplitudes, and thus the current characteristics to which the battery cells are exposed to. High-resolution histograms are impractical to work with when the current patterns are being assessed manually, as well as the profile dynamic compositions. They can be simplified by reducing their resolution; in this specific example, we have separated the currents into five bins, separately for charging and discharging. The charging current exhibits a trend, where the higher the amplitude the lower the occurrence. The occurrences of the discharging current amplitudes have a more complex character. The first bin (the lowest discharging current) is experienced over a major amount of time (for the investigated satellites it is about 0.66–0.82 fraction of time). The second current amplitude bin has the occurrence three-four times less than the first bin. Regarding the high current discharge, GOMX-3 shows nearly no discharging current belonging to bins 3–5. GOMX-4 satellites show a distinguishable occurrence of the 4th bin, while the 3rd and 5th are very low. Thus, it can be approximated that there are three significant amplitudes of the discharging current: low = 1st bin, medium = 2nd bin, and high = amplitude of the 4th bin, with the sum occurrences of the 3rd, 4th and 5th bins. Examples of current at various orbits and the grouping procedure is illustrated in Fig. 5 a) and b).

From the current telemetry analysis via histograms, the current ($\mathbf{I}_{\mathrm{x,h,i}}$) and the current occurrence ratio ($\mathbf{R}_{\mathrm{x,h,i}}$) vectors are formed for each satellite. Since charging and discharging vectors have an identical length across the satellites, their aggregated values ($\langle\mathbf{I}_{\mathbf{x,h}}\rangle_{\mathrm{sat}}$, $\langle\mathbf{R}_{\mathbf{x,h}}\rangle_{\mathrm{sat}}$), representing a group of satellites, can be determined according to (1) and (2). The individual current and ratio values for each satellite and their aggregated values are shown in Fig. 5 c). An average charging/discharging current in an orbit ($\langle I_{\mathrm{x,h}}\rangle_{\mathrm{sat,orbit}}$) can be determined from $\langle\mathbf{I}_{\mathbf{x,h}}\rangle_{\mathrm{sat}}$ and $\langle\mathbf{R}_{\mathbf{x,h}}\rangle_{\mathrm{sat}}$ via (3), and it is used to obtain the normalized aggregated current values ($\langle\mathbf{I}_{\mathbf{x,n}}\rangle_{\mathrm{sat}}$), as described in (4). At this moment, current characteristics, representing a specific group of satellites, are derived in means of a normalized aggregated current vector $\langle\mathbf{I}_{\mathbf{x,n}}\rangle_{\mathrm{sat}}$ and their occurrence ratios $\langle\mathbf{R}_{\mathbf{x,h}}\rangle_{\mathrm{sat}}$.

$$\langle\mathbf{I}_{\mathbf{x,h}}\rangle_{\mathrm{sat}} = \frac{\sum_{i=1}^{n}\mathbf{I}_{\mathrm{x,h,i}}}{n} \tag{1}$$

$$\langle\mathbf{R}_{\mathbf{x,h}}\rangle_{\mathrm{sat}} = \frac{\sum_{i=1}^{n}\mathbf{R}_{\mathrm{x,h,i}}}{n} \tag{2}$$

$$\langle I_{\mathrm{x,h}}\rangle_{\mathrm{sat,orbit}} = \langle\mathbf{I}_{\mathbf{x,h}}\rangle_{\mathrm{sat}} \times \langle\mathbf{R}_{\mathbf{x,h}}\rangle_{\mathrm{sat}}^{\mathsf{T}} \tag{3}$$

$$\langle\mathbf{I}_{\mathbf{x,n}}\rangle_{\mathrm{sat}} = \frac{\langle\mathbf{I}_{\mathbf{x,h}}\rangle_{\mathrm{sat}}}{\langle I_{\mathrm{x,h}}\rangle_{\mathrm{sat,orbit}}} \tag{4}$$

2) Current mission profile synthesis: To derive a specific SMP, $\langle\mathbf{I}_{\mathbf{x,n}}\rangle_{\mathrm{sat}}$ has to be scaled by the target orbit and test characteristics. Required orbit characteristics are considered to be the orbit time (τ_{orbit}), the fractional duration of eclipse in relation to the orbit time (E_{r}), and the lag variable (L_{r}). τ_{orbit} started for GOMX-3 at 5556 seconds and it decayed over the life of one year to 5290 seconds. For GOMX-4, the τ_{orbit} value is around 5669 seconds and it shows a very small linear decrement over a year. A generic LEO τ_{orbit} is defined in the ESA handbook as 5400 seconds [3] and this value is selected further on for deriving of an example SMP. The E_{r} values have been approximately 0.39 for GOMX-3 and 0.31 for GOMX-4. A generic value specified by the ESA handbook is 0.33 [3] and it is as well used further on. L_{r} represents a possible 'lag' between entering/leaving the sun light and starting/stopping to charge the batteries, which depends on power generation and consumption balance. Consequently, it affects duration of charging/discharging periods. There are two special cases that can occur. When $L_{\mathrm{r}} = 0$, then charging/discharging times are determined solely from E_{r}. In that case, $E_{\mathrm{r}} = 0.33$ results into the charging time $\hat{\tau}_{\mathrm{c}}$ to be two times longer than discharging

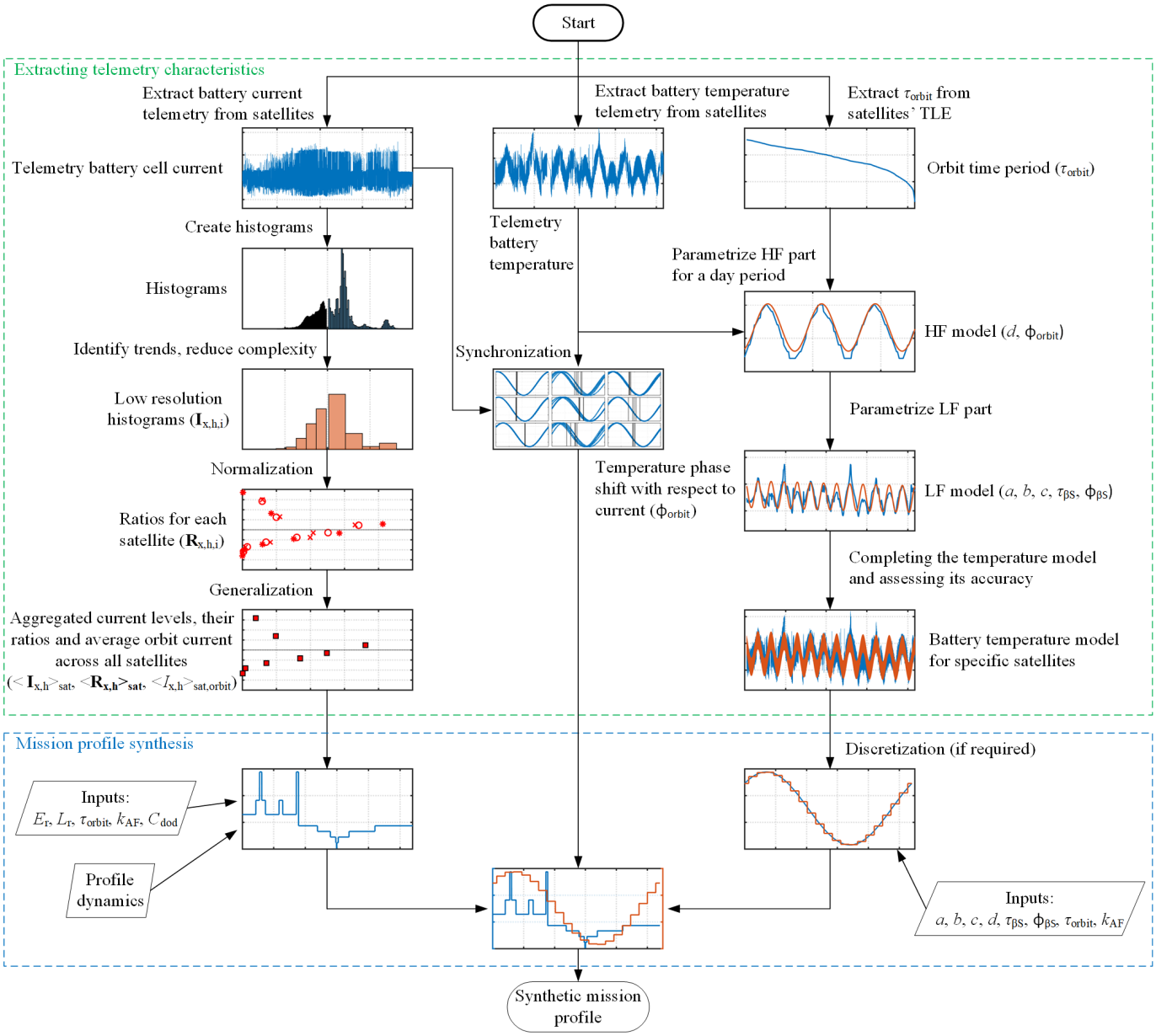

Fig. 3. Flowchart illustrating the proposed methodology to determine a SMP.

time $\hat{\tau}_{\mathrm{d}}$. On the other hand, when $E_{\mathrm{r}}+L_{\mathrm{r}}=0.5$, which in this example means $L_{\mathrm{r}}=0.17$, then $\hat{\tau}_{\mathrm{c}}$ and $\hat{\tau}_{\mathrm{d}}$ are equal. Since the general aim is to have same amount of capacity charged and discharged during an orbit, $\hat{\tau}_{\mathrm{c}}$ and $\hat{\tau}_{\mathrm{d}}$ determines the required current rates.

For test purposes, an accelerating factor (k_{AF}) is introduced. A SMP standard time length with $k_{\mathrm{AF}}=1$ is τ_{orbit}. However, sometimes for test purposes, it is required to accelerate tests (e.g. cycle lifetime testing). The SMP time duration can be then inversely proportional shortened according to k_{AF}. Thus, the respective charging/discharging times ($\hat{\tau}_{\mathrm{x}}$) can be obtained from (5).

$$\hat{\tau}_{\mathrm{x}}=\begin{cases}\tau_{\mathrm{orbit}}[1-(E_{\mathrm{r}}+L_{\mathrm{r}})/k_{\mathrm{AF}}], & \text{for charging}\\ \tau_{\mathrm{orbit}}[(E_{\mathrm{r}}+L_{\mathrm{r}})/k_{\mathrm{AF}}], & \text{for discharging}\end{cases} \tag{5}$$

Another important mission design parameter is the DOD, which batteries are going to experience. Generally, smaller values of DOD (i.e. 10–40%) are selected for Li-ion batteries in LEO satellites, to allow for a sufficient cycle life (approximately 5500 cycles per year at LEO) [41]. The DOD specifies the capacity that is to be charged/discharged during one orbit (C_{dod} in Ampere-seconds). With the determined DOD and charging/discharging times, the average charging/discharging current of the specific SMP ($\langle\hat{I}_{\mathrm{x}}\rangle_{\mathrm{orbit}}$) can be derived from (6).

$$\langle\hat{I}_{\mathrm{x}}\rangle_{\mathrm{orbit}}=\frac{C_{\mathrm{dod}}}{\hat{\tau}_{\mathrm{x}}} \tag{6}$$

The average SMP charging/discharging current is then used to scale the normalized aggregated current vector to obtain the specific current values for the SMP ($\hat{\mathbf{I}}_{\mathrm{x}}$), as shown in (7). The

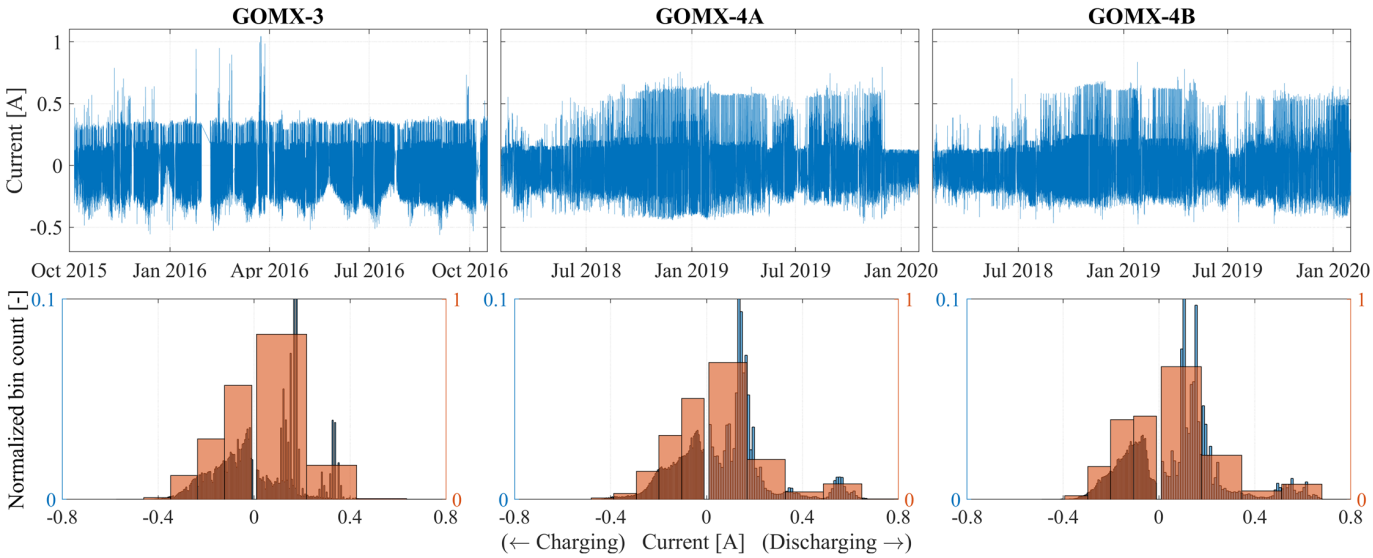

Fig. 4. The battery cell current telemetry data and it's representation in a form of histograms (blue for a high resolution, red for a reduced resolution).

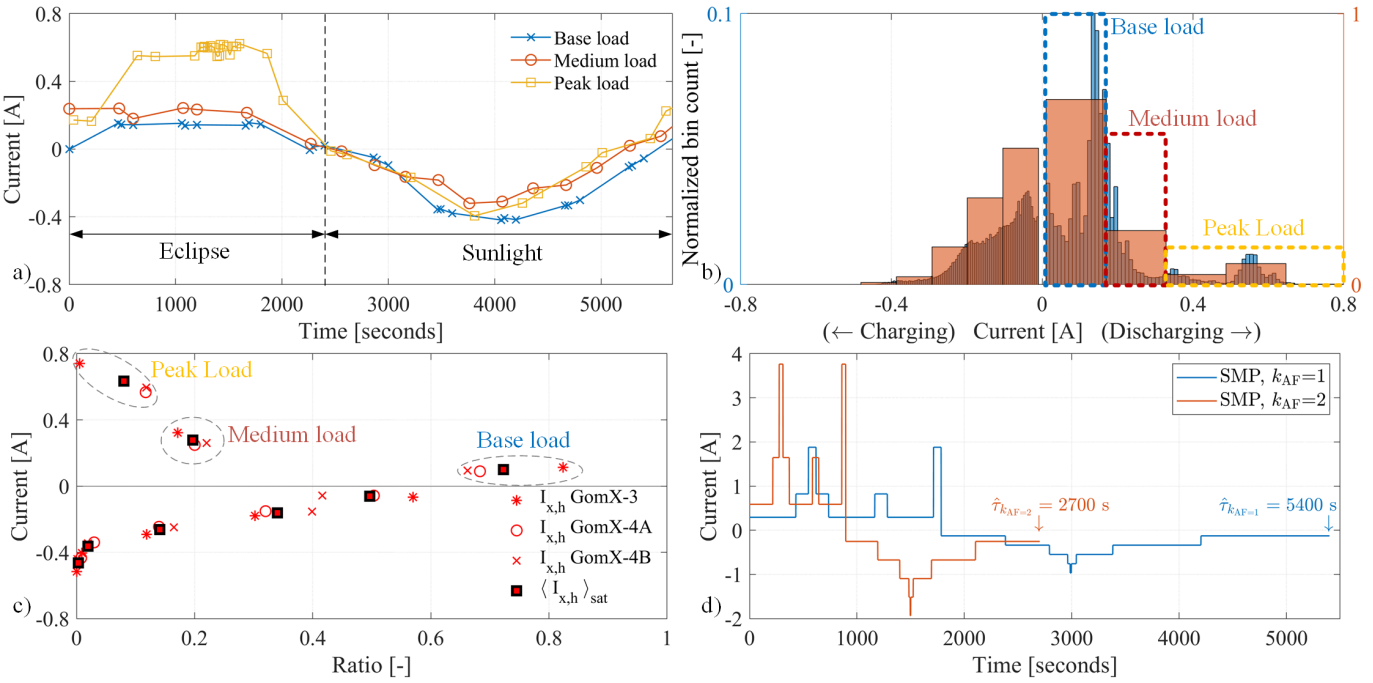

Fig. 5. Illustration of steps leading to a synthetic mission profile: a) current pattern examples during an orbit for GOMX-4A; b) current histograms and their division to three load levels in a case of GOMX-4A; c) charging and discharging currents and their relative occurrence for GOMX satellites and their resulting average values; d) Derived SMPs for various accelerating factors and DOD = 10%.

term contains also a variable $\eta_{\mathrm{I,x}}$ that stands for Coulombic efficiency, and it allows to account for charging/discharging efficiency and losses of a Li-ion battery cell, a battery pack, and/or of an electrical power supply. The specific values considered in this work are $\eta_{\mathrm{I,c}} = 0.95$ and $\eta_{\mathrm{I,d}} = 1$.

$$\hat{\mathbf{I}}_{\mathrm{x}} = \langle \hat{I}_{\mathrm{x}} \rangle_{\mathrm{orbit}} \cdot \langle \mathbf{I}_{\mathbf{x},\mathbf{n}} \rangle_{\mathrm{sat}} \cdot \eta_{\mathrm{I,x}} \tag{7}$$

At this stage, currents amplitude vector for the SMP is determined and it remains to form its dynamic profile. It was observed that a frequent characteristic of the charging current profile is that it sharply increases in approximately 1/3 of sunlight time and then it slowly decreases for approximately 2/3 of the time. Thus a similar proportional profile is composed. For the discharging current profile, there is no specific lead of how it should be composed, since the telemetry resolution was too crude to capture detailed dynamics and the load periods often exhibited a constant current trend. Subsequently, it is considered that the test profile should be simple enough, while beneficial for further use and representing the worst case scenario. If the loading order will be only the base load, the medium load and the peak load, a lot of information about battery and its dynamic can be lost. Therefore, an

indented profile was chosen, where one can find various transitions between current amplitudes. This profile addresses the worst case scenario, as it includes the peak load at the end of discharge (a placement, where the lowest SOC will be reached, thus the highest chance to trigger the discharging safety voltage limit). The SMP profile for various k_{AF} is illustrated in Fig. 5 d). As alternative procedure, an energy management scheduling [34] can be taken in account to form the discharging profile. At the end, for practical reasons, it is convenient to round the current values (depending on the range of a test device, typically two decimals).

B. Temperature

From a thermal perspective, the battery temperature is a result of the internal heat generation and the external heat exchange. The external heat exchange for the batteries means the exchange with the rest of the spacecraft, where the satellite subsystems typically contribute to the heat generation and heat is also exchanged with the environment.

The temperature telemetry data was collected from three satellites: GOMX-3 (from 5.10.2015 to 17.10.2016), GOMX-4A (from 15.11.2018 to 31.1.2020) and GOMX-4B (from 10.05.2019 to 31.1.2020) and it is shown in Fig. 7 (the top row).

1) Temperature telemetry analysis: From the telemetry, it is observed that the batteries in GOMX-3 experienced large temperature fluctuations during the mission. Due to the heaters having not set automatic activation, the batteries' temperature dropped below zero for approximately 10% of the mission duration, and the minimum temperature was -12 °C. Generally, COTS Li-ion batteries do not perform well at low temperatures, and it can also affect their lifetime. However, in this case, the low temperature does not cause any battery performance limitations. Moreover, the charging current was nearly the whole time below 0.4 A (∼0.15 C-rate), and the value of average charging current was 0.16 A (∼0.06 C-rate), which can be considered as sufficiently low, since no pronounced degradation was observed, and the batteries performed well during this one-year mission. Temperature variations were much less for GOMX-4 CubeSats during the observed period. Due to thermal design, GOMX-4B has a lower spacecraft temperature, and when the battery temperature drops below zero, the heaters are activated. That has occurred very rarely during the observed period (33 incidences) and it has not affected an overall trend tendency significantly. Furthermore, there has not been a high-power loading of the batteries at all the spacecrafts that would cause a significant self-heating. Thus, it can be considered that the major influence on the battery temperature fluctuations is coming from the orbital mechanics of the spacecrafts.

The low frequency fluctuations can be explained by the time exposure to the Sun during a single orbit (a fraction between sunlight and eclipse). Longer sunlight periods mean that the spacecraft gets heated more during an orbit and vice-versa. The lasting of the eclipse is determined by the angle between the Sun and the orbital plane (β_S angle) and it changes according to the orbit inclination. GOMX-3 was launched from the ISS with an inclination of 51.6°, which results into pronounced changes in the β_S throughout the year. On the other hand, GOMX-4, having SSO, experiences only a minor variations of the β_{S} throughout the year.

The high frequency fluctuations, illustrated as a detail for GOMX-4B in Fig. 7, correspond to individual orbit revolutions. The eclipse of the individual orbit revolution is determined from the low frequency fluctuations and β_{S} mentioned above. The orbit period is related to the altitude of the orbit and it is shown in Fig. 6. While GOMX-3 orbit period decayed significantly during the year, before it made a re-entry, GOMX-4 orbit period has changed very little (2 seconds over one year).

The proposed temperature model is presented in (8). It is split into two parts, according to the scale of their dynamics. The first part describes the low frequency (LF) behavior. The temperature signal has an offset value, a, which expresses the middle temperature value in the beginning of a mission. This middle temperature value was observed to be decreasing over the mission time. This decrease is considered to be linked with the altitude decay of the satellite and by it with a decrease in the orbit time period, as it is visualized in Fig. 7. Thus, a linear expression, characterized by a slope b, was considered as a suitable approximation to capture this decay. Then, approximately sinusoidal oscillations occur at a LF scale, that are related to changes in β_{S} throughout the year. The parameter c is describing the amplitude of this LF sinusoidal oscillations, $\tau_{\beta_{\mathrm{S}}}$ is a period of these oscillations and $\phi_{\beta_{\mathrm{S}}}$ is the phase shift. The second part describes the high frequency (HF) temperature dynamics related to a single orbit revolution, which have also a sinusoidal oscillating character. The parameter d stands there for the amplitude, τ_{orbit} for an orbit time period and ϕ_{orbit} for the HF phase shift.

$$T = \underbrace{a + b \cdot t + c \cdot \sin\left(\frac{2 \cdot \pi \cdot t}{\tau_{\beta_{\mathrm{S}}}} + \phi_{\beta_{\mathrm{S}}}\right)}_{\text{Low Frequency (LF)}} + \underbrace{d \cdot \sin\left(\frac{2 \cdot \pi \cdot t}{\tau_{\mathrm{orbit}}} + \phi_{\mathrm{orbit}}\right)}_{\text{High Frequency (HF)}} \quad (8)$$

The model parameters can be found via non-linear least square regression applied to the telemetry data, shown in Figure 7 in the top row. However, to fit all data at once is a too complex task, due to noise in the data, and the fact that the model is a simplification of a complex behavior, and it does not capture all the aspects. Thus, for simplicity, the parameter fitting procedure is split into two steps according to the respective frequency ranges. For the LF fitting, the HF data can be treated as a noise. Thus, a temperature daily average is determined at first. In order to obtain approximately one day long data segments, the telemetry data are split into sets with 16 and 15 consecutive orbits for GOMX-3 and GOMX-4, respectively. The resulting daily average is shown in Figure 7 in the second row. The daily average is then fitted to the LF part of the model.

TABLE I
TEMPERATURE MODEL FITTED PARAMETERS

Parameter	a [°C]	b [°C/day]	c [°C]	d [°C]	τ_{β_S} [days]	ϕ_{β_S} [°]	RMSE [°C]
GOMX-3	12.56	-1.34×10^{-12}	10.00	6.78	29.43	139.23	6.35
GOMX-4A	21.08	-9.49×10^{-13}	2.57	2.54	358.07	118.98	1.87
GOMX-4B	14.44	-1.36×10^{-12}	4.35	3.53	360.00	121.20	1.92

The obtained parameters are shown in Table I, and the LF model output is presented in Figure 7 in the third row. For parametrization of the HF model, the LF variations can be treated as an offset. Subsequently, by removing the daily average from the day-segments, the HF parameters can be found directly by fitting the HF model. The fitted d values exhibit only negligible variations throughout the considered mission interval, suggesting to use its mean value as its representative, presented in Table I. The fitted ϕ_{orbit} shows a periodic character. MATLAB's function $unwrap$ was used to obtain its value in terms of time series over the whole mission time interval.

The output of the resulting model (LF+HF) is shown in Fig. 7 in the bottom row. The root-mean-square-error (RMSE) between the model and the telemetry is 6.35, 1.87 and 1.92 °C for GOMX-3, GOMX-4A and GOMX-4B, respectively. A considerable contribution to the RMSE is the not perfectly matching phase shift ϕ_{orbit}. Even though the fitted ϕ_{orbit} for one day data provides a very good match, when it is used as a look-up table (i.e., ϕ_{orbit} versus t), it can cause the model to diverge from the telemetry data at some places due to not perfectly aligned phase shift. For shorter time periods, ϕ_{orbit} can be determined more accurately. When only the thermal profile is considered, ϕ_{orbit} can be neglected, otherwise when it is used in relation to current, the corresponding phase shift is addressed in section IV-C. Regarding the higher RMSE for GOMX-3, variations of β_S were only approximated by the sine function, and this simplification does not allow for a perfect match.

2) Temperature mission profile synthesis: For a laboratory application, it can be considered to use the complete model (8), or only its HF part, if a scale of one orbit is of the interest. The model parameters are selected to represent the desired scenario (e.g. cold case, hot case). Moreover, k_{AF} can be applied as well to the temperature model, to create an 'accelerated' output signal. For the implementation in the laboratory testing, it might be necessary to discretize the continuous sine based profile in order to control temperature by simple steps.

3) Sensitivity of the temperature model on parametrization time periods: Since different time periods of data can be available for identifying parameters in (8), their variations are explored on GOMX-3 telemetry, which is considered to be a highly challenging scenario compared to GOMX-4 regarding the temperature dynamics. The model in (8) was parametrized using 1, 3, 6, and 9 months periods from the total of 12 months worth of GOMX-3 data. Subsequently, the model predictions are illustrated in Fig. 8, and the identified parameters, including the model error for the whole period, are presented in Table II. The 12 months period, in this case, meaning the parametrization applied to all data, can be considered as a target. It is observed that even one month

TABLE II
TEMPERATURE MODEL PARAMETERS FOR GOMX-3, WHEN USING VARIOUS TIME INTERVALS FOR ITS PARAMETRIZATION.

Parameter	a [°C]	b [°C/day]	c [°C]	d [°C]	τ_{β_S} [days]	ϕ_{β_S} [°]	RMSE [°C]
1 month	11.70	7.32×10^{-12}	10.00	6.15	30.00	156.18	17.02
3 months	11.30	2.86×10^{-12}	10.00	6.57	29.12	143.11	11.57
6 months	12.65	-1.02×10^{-12}	10.00	6.82	29.68	149.34	7.76
9 months	13.72	-2.79×10^{-12}	10.00	6.77	29.66	149.73	7.08
12 months	12.56	-1.34×10^{-12}	10.00	6.78	29.43	139.23	6.35

period for parametrization was enough to obtain sufficiently close parameters to the target, except the parameter b, that describes a slow, long-term shift. Due to b is being inaccurately identified, positive instead of negative, for 1 month and 3 months periods, the model predictions result in diverging from telemetry, and consequently, they achieve a larger RMSE of 17.02 and 11.57 °C, respectively. Meanwhile, the predictions based on 6 and 9 months parametrization periods got an RMSE 7.76 and 7.08 °C, respectively, which is close to the base case value 6.35 °C. Thus, in the case of GOMX-3 mission, which started on ISS orbit, it is considered that it is required at least 6 months period to parametrize the full temperature model that provides sufficient accuracy for a yearly period.

Only the HF part of the temperature model (8) can be considered to capture orbit-to-orbit or day-to-day temperature variations on a short scale. Subsequently, one day period ($\sim$16 orbits) was used to parametrize the model for GOMX-3 and it was used for a short-term one-week prediction, illustrated in Fig. 9. The prediction holds well for 1–2 days; however afterward, the predicted temperature starts to diverge due to the LF dynamics that were omitted. For the profiles with flatter dynamics, such as GOMX-4, the predictions are valid for longer periods.

C. Synchronizing the profiles

To have temperature and current profiles appropriately coupled, they have to be time-wise synchronized, i.e. temperature experiencing during charging shall be happening when charging current is applied and vice versa. Following the convention determined from the current profile (i.e., that discharging is first and charging comes afterward), the temperature profile has to have corresponding phase shift. In order to find a general trend, five orbits were selected from the beginning, middle and ending period of the available data for each satellite. The beginning of charging/discharging was detected based on change of battery current sign. Five such orbits selected for GOMX-3 are illustrated in Fig. 10, including battery current, solar generated current, telemetry temperature, and temperature fitted according to the model.

The next step was to separate the individual orbits and to normalize their time base. In that way, the individual orbits can be plotted over each other, as illustrated in Fig. 11. There are three features that can be used to describe a shift of the temperature profile: time of the maximum peak, time of the beginning of charging, time of the minimum peak. Their average values over the five orbits are presented in Table III. The values slightly vary throughout the mission. There is a significant change for the ending period of GOMX-3 that might be caused by its pronounced decay in altitude, resulting

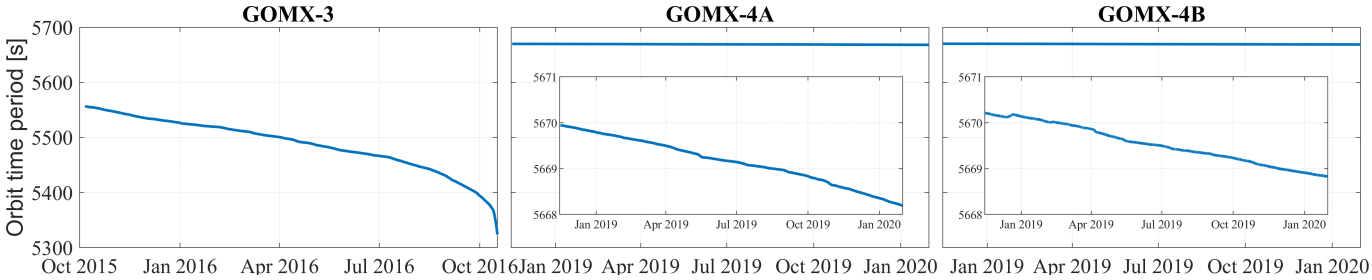

Fig. 6. Orbit time period that is shortened with a decay in satellite altitude.

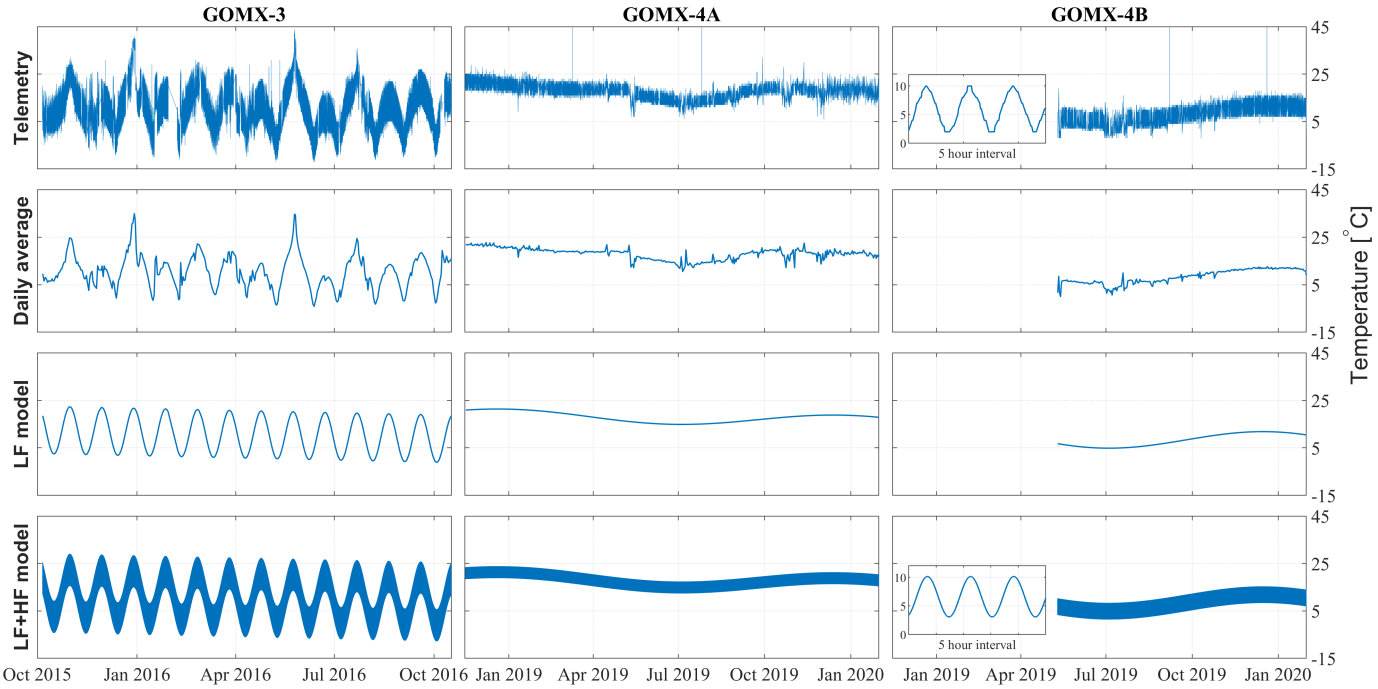

Fig. 7. Satellite temperature telemetry and model outputs. The character of temperature variations is determined by the character of satellite's orbit (ISS orbit for GOMX-3, SSO for GOMX-4).

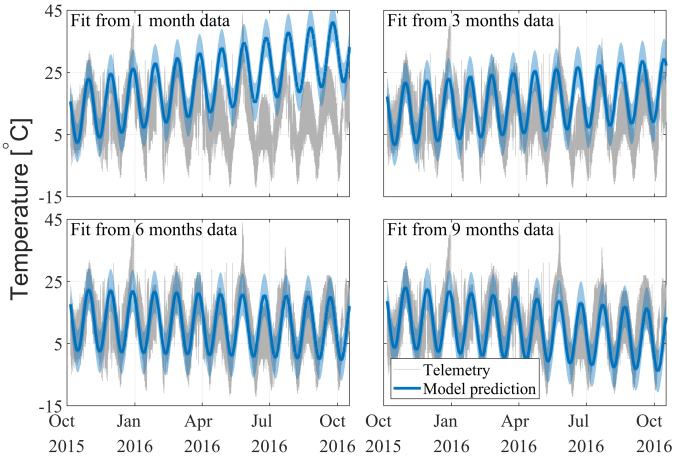

Fig. 8. The model predictions according to various time intervals used for its parametrization.

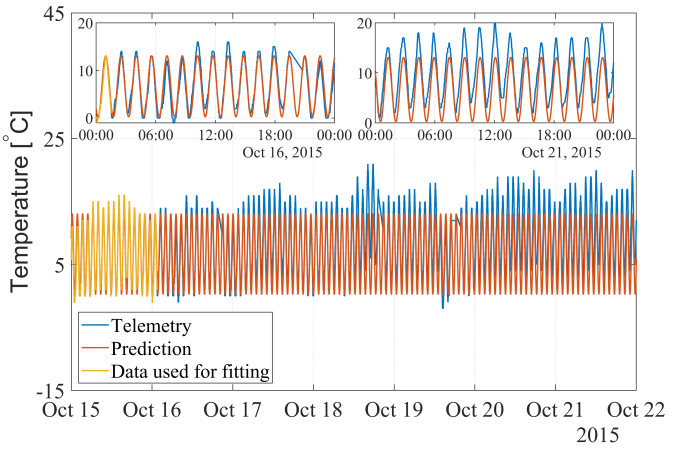

Fig. 9. The temperature model prediction for one week based on one day parametrization for GOMX-3, with a detail of the first and the last predicted day in the selected period.

in a shorter orbit time period (see Fig.6). The normalized time of beginning of charging corresponds to the term $E_r + L_r$ in (5). For GOMX-3, the beginning of charging in the beginning and the middle periods corresponds to the considered E_r and it is around 0.39. For GOMX-4, the beginning of charging is between 0.4 and 0.55, which is more than the considered $E_r = 0.31$. Thus, the 'lag' L_r, discussed in section IV-A,

TABLE III
FEATURE POSITIONS IN TEMPERATURE THROUGHOUT ORBITS

Parameter	Maximum peak			Beginning of charging			Minimum peak		
Period	B	M	E	B	M	E	B	M	E
GOMX-3	0.03	0.05	0.14	0.40	0.39	0.55	0.53	0.55	0.64
GOMX-4A	0.16	0.21	0.15	0.52	0.55	0.40	0.67	0.72	0.65
GOMX-4B	0.10	0.19	0.17	0.41	0.50	0.49	0.60	0.69	0.66
Mean	0.13			0.47			0.63		

*B - beginning, M - middle, E - ending

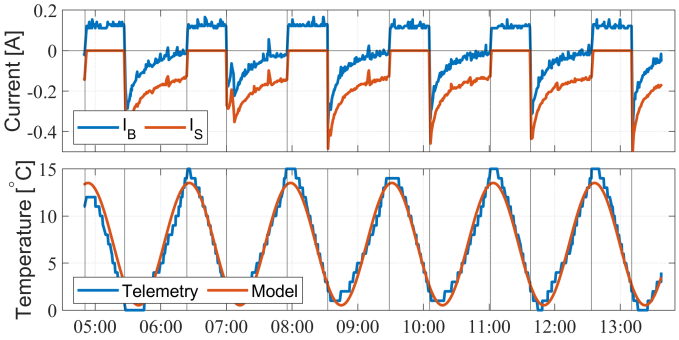

Fig. 10. Five selected GOMX-3 orbits with marked beginning of charging and discharging periods (black vertical lines). 15th October 2015

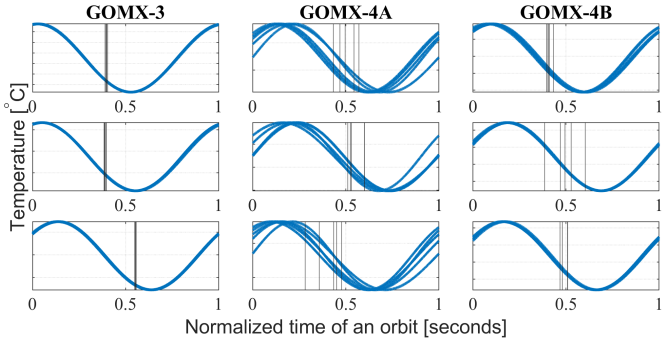

Fig. 11. Temperature profiles plotted in an overlapping manner for five orbits from the beginning period (1st row), the middle period (2nd row) and the ending period (3rd row) of available telemetry data. The vertical lines mark the detected beginning of charging.

is present, ranging in 0.09–0.24. To generalize, the battery temperature reaches its maximum value shortly after beginning of discharging, and it arrives to the lowest value after the charging started. The representative normalized time values for maximum peak, beginning of charging, and minimum peak are 0.13, 0.47, and 0.63, taken as an average across the satellites. Since the maximum and the minimum peaks would occur at 0.25 and 0.75, respectively, of the normalized time at a sine wave without any phase shift, the phase shift of the temperature profile with respect to the current profile, expressed in degrees, can be computed as shown in (9). The corresponding synchronized profile is illustrated in Fig. 12.

$$\phi_{\text{orbit}} = (0.25 - 0.13) \cdot 360^\circ = 43.2^\circ \tag{9}$$

V. Experimental

Since the derived SMPs are dedicated for on-ground battery testing and simulations, they are actually demonstrated via laboratory measurements. The tests were performed on 3.0 Ah Li-ion battery cells, and C_{DOD} was selected to be 0.3 Ah for a corresponding cycle depth of 10%. A Digatron BTS 600 battery test station was used for the constant temperature

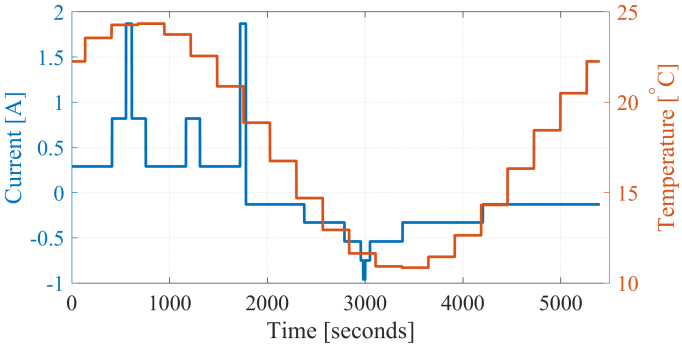

Fig. 12. Synchronized current and temperature SMP for $C_{\text{DOD}} = 0.26$Ah, $k_{\text{AF}} = 1$, LF $= 17.6$ °C, $d = 6.8$ °C, $\phi_{\text{orbit}} = 43.2°$.

SMP testing, and MACCOR Series 4000 battery test station was used for the variable temperature SMP testing. Battery charging is limited to 4.0 V, similarly as it would be in a CubeSat, to avoid excessive degradation due to the fully charging of the cells. Prior to the tests, the cells were charged with 1.5 A constant current to the voltage limit (i.e., 4.0 V), and then by constant voltage charging until the current dropped to 50 mA.

To visualize the measurements, only the first five cycles are used. The SMP with constant temperature profile is shown in Fig. 13, and the SMP with the variable temperature profile is shown in Fig. 14. The orbit (cycle) time is in the test accelerated according to their k_{AF}. The used k_{AF} has also an effect on the current amplitude: the shorter the test time, the higher the current amplitude. The voltage and current responses of the cells are as expected, except two phenomena. The cells are initially charged to limits of 4.0 V and 50 mA. During the SMP cycling, the voltage limit is set to 4.0 V as well. Thus, the charging current can be reduced in order to not exceed this voltage limit, resulting in less capacity to be charged. A similar thing would occur as well at a CubeSat, when charging is controlled by voltage. This leads to a slight drift in SOC over multiple cycles, until the drift is eliminated by reaching the situation, when the charging current is never reduced. The drift can be prevented in the test by increasing the current limitation of the constant voltage charging phase from 50 mA to a higher value. The second noticeable difference in Fig. 14 are 'spikes' in voltage and current. This is the result of the temperature control of the climatic chamber, where the experiments were carried out. When the temperature set-point is changing, the test station pauses the current, and this current interruption causes a voltage response. However, the interruption occurs only in a range of seconds, and it does not have a further consequence on the test, it is rather an artifact of the practical implementation in this case.

VI. Conclusion and Future Work

Realistic mission profiles are an important part of technology proofing and validation. They are widely established and used in the automotive industry, but they are missing in many niche areas such as the case of space industry and CubeSats. Thus, this work is filling the scientific gap and provides the

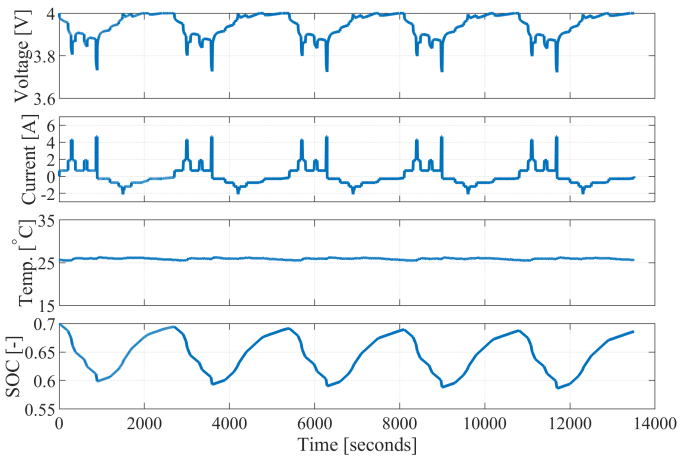

Fig. 13. Measured SMP for $C_{\mathrm{DOD}} = 0.3$Ah, $k_{\mathrm{AF}} = 2$, LF $= 25$ °C, $d = 0$ °C (constant temperature).

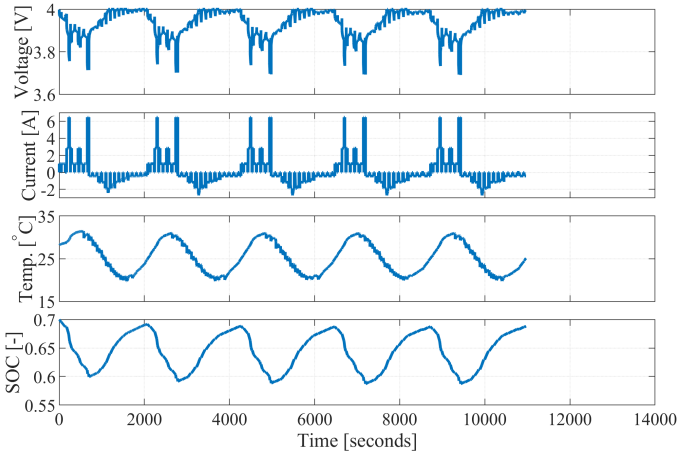

Fig. 14. Measured SMP for $C_{\mathrm{DOD}} = 0.3$Ah, $k_{\mathrm{AF}} = 3$, LF $= 25$ °C, $d = 7$ °C, $\phi_{\mathrm{orbit}} = 30.4°$.

first step, which can lead to future test standardization for the batteries in CubeSats.

Telemetry data from three CubeSats were analyzed and used for modelling of current and temperature mission profiles. The proposed methodology to derive these representative mission profiles was designed in an open way, in order that every step can be further refined, and as well more field data can be provided as an input. The current SMP is created with consideration of specific application characteristics and it is well suitable for real time and also accelerating battery testing. The formulated temperature model describes closely the battery temperature throughout the mission, and it is used to derive the temperature SMP. Then, the synchronized current and temperature SMPs are representative for the battery use in CubeSats, as they properly capture charging and discharging periods occurring at corresponding temperature levels.

The aspects of a constant temperature testing versus a variable temperature testing were already demonstrated for SOC estimation in our previous work [42]. The future work will focus on degradation analysis and differences between a classical CC-CV cycling, and using current and temperature SMP, as the specific SMP profiles were presented in this manuscript. Moreover, pattern recognition algorithms will be used in processing the telemetry, and to determine current dynamics in mission profiles in order to reach higher level of generalization and automation of the process.

REFERENCES

[1] S. DelPozzo and C. Williams, "Nano/Microsatellite Market Forecast, 10th Edition," Tech. Rep., 2020.

[2] A. Poghosyan and A. Golkar, "CubeSat evolution: Analyzing CubeSat capabilities for conducting science missions," *Progress in Aerospace Sciences*, vol. 88, no. September 2016, pp. 59–83, jan 2017.

[3] ESA-ESTEC, "Space engineering Li-ion battery testing handbook (ECSS-E-HB-20-02A)," pp. 1–31, 2015.

[4] X. Wang, Y. Sone, and S. Kuwajima, "Effect of operation conditions on simulated low-earth orbit cycle-life testing of commercial lithium-ion polymer cells," *Journal of Power Sources*, vol. 142, no. 1-2, pp. 313–322, mar 2005.

[5] T. Motohata, T. Shimizu, H. Masui, and M. Cho, "Development of a Testing Standard of COTS Lithium-Ion Batteries for Nano-Satellite," in *65th International Astronautical Congress (IAC)*, 2014.

[6] S. Brown, K. Ogawa, Y. Kumeuchi, S. Enomoto, M. Uno, H. Saito, Y. Sone, D. Abraham, and G. Lindbergh, "Cycle life evaluation of 3Ah LixMn2O4-based lithium-ion secondary cells for low-earth-orbit satellites," *Journal of Power Sources*, vol. 185, no. 2, pp. 1444–1453, dec 2008.

[7] J.-W. Lee, Y. K. Anguchamy, and B. N. Popov, "Simulation of charge–discharge cycling of lithium-ion batteries under low-earth-orbit conditions," *Journal of Power Sources*, vol. 162, no. 2, pp. 1395–1400, nov 2006.

[8] X. Wang, C. Yamada, H. Naito, and S. Kuwajima, "Simulated low-earth-orbit cycle-life testing of commercial laminated lithium-ion cells in a vacuum," *Journal of Power Sources*, vol. 140, no. 1, pp. 129–138, jan 2005.

[9] D. Wong, B. Shrestha, D. A. Wetz, and J. M. Heinzel, "Impact of high rate discharge on the aging of lithium nickel cobalt aluminum oxide batteries," *Journal of Power Sources*, vol. 280, pp. 363–372, apr 2015.

[10] Y. Gao, J. Jiang, C. Zhang, W. Zhang, Z. Ma, and Y. Jiang, "Lithium-ion battery aging mechanisms and life model under different charging stresses," *Journal of Power Sources*, vol. 356, pp. 103–114, jul 2017.

[11] B. Epding, B. Rumberg, H. Jahnke, I. Stradtmann, and A. Kwade, "Investigation of significant capacity recovery effects due to long rest periods during high current cyclic aging tests in automotive lithium ion cells and their influence on lifetime," *Journal of Energy Storage*, vol. 22, no. December 2018, pp. 249–256, apr 2019.

[12] V. Giuliani and S. Remy, "Qualification of a modular Li-ion battery pack for LEO Satellites based on cells not specifically designed for space applications," in *2019 European Space Power Conference (ESPC)*. IEEE, sep 2019, pp. 1–9.

[13] R. W. Cook, L. G. Swan, and K. P. Plucknett, "Failure mode analysis of lithium ion batteries operated for low Earth orbit CubeSat applications," *Journal of Energy Storage*, vol. 31, no. February, p. 101561, 2020.

[14] R. Cook, L. Swan, and K. Plucknett, "Impact of Test Conditions While Screening Lithium-Ion Batteries for Capacity Degradation in Low Earth Orbit CubeSat Space Applications," *Batteries*, vol. 7, no. 1, p. 20, mar 2021.

[15] B. Saha and K. Goebel, "Battery Data Set," 2007. [Online]. Available: http://ti.arc.nasa.gov/project/prognostic-data-repository

[16] B. Yu, T. Zhang, T. Liu, and L. Yao, "Reliability Evaluation and In-Orbit Residual Life Prediction for Satellite Lithium-Ion Batteries," *Mathematical Problems in Engineering*, vol. 2018, pp. 1–12, dec 2018.

[17] H. Aung and K. S. Low, "Temperature dependent state-of-charge estimation of lithium ion battery using dual spherical unscented Kalman filter," *IET Power Electronics*, vol. 8, no. 10, pp. 2026–2033, oct 2015.

[18] H. Aung, J. J. Soon, S. T. Goh, J. M. Lew, and K.-S. Low, "Battery Management System With State-of-Charge and Opportunistic State-of-Health for a Miniaturized Satellite," *IEEE Transactions on Aerospace and Electronic Systems*, vol. 56, no. 4, pp. 2978–2989, aug 2020.

[19] L. Slongo, S. Martínez, B. Eiterer, T. Pereira, E. Bezerra, and K. Paiva, "Energy-driven scheduling algorithm for nanosatellite energy harvesting maximization," *Acta Astronautica*, vol. 147, no. May 2017, pp. 141–151, jun 2018.

[20] T. Totani, H. Ogawa, R. Inoue, T. K. Das, M. Wakita, and H. Nagata, "Thermal Design Procedure for Micro- and Nanosatellites Pointing to Earth," *Journal of Thermophysics and Heat Transfer*, vol. 28, no. 3, pp. 524–533, jul 2014.

[21] S. Ma, M. Jiang, P. Tao, C. Song, J. Wu, J. Wang, T. Deng, and W. Shang, "Temperature effect and thermal impact in lithium-ion batteries: A review," *Progress in Natural Science: Materials International*, vol. 28, no. 6, pp. 653–666, dec 2018.

[22] S. Tippmann, D. Walper, L. Balboa, B. Spier, and W. G. Bessler, "Low-temperature charging of lithium-ion cells part I: Electrochemical modeling and experimental investigation of degradation behavior," *Journal of Power Sources*, vol. 252, pp. 305–316, apr 2014.

[23] C. Yan, Y.-X. Yao, W.-L. Cai, L. Xu, S. Kaskel, H. S. Park, and J.-Q. Huang, "The influence of formation temperature on the solid electrolyte interphase of graphite in lithium ion batteries," *Journal of Energy Chemistry*, vol. 49, pp. 335–338, oct 2020.

[24] V. Knap, L. K. Vestergaard, and D.-i. Stroe, "Towards Validation of Battery Mission Lifetime for Nano-satellites: Fast, Cheap and Accurate Through a Representative Mission Profile," in *2019 European Space Power Conference (ESPC)*. IEEE, sep 2019, pp. 1–5.

[25] D. Selva and D. Krejci, "A survey and assessment of the capabilities of Cubesats for Earth observation," *Acta Astronautica*, vol. 74, pp. 50–68, 2012.

[26] GomSpace A/S, "3U nanosatellite will provide daily coverage of Colombian territory," accessed 14.11.2019. [Online]. Available: https://gomspace.com/facsat.aspx

[27] E. Peral, S. Tanelli, Z. Haddad, O. Sy, G. Stephens, and E. Im, "Raincube: A proposed constellation of precipitation profiling radars in CubeSat," *International Geoscience and Remote Sensing Symposium (IGARSS)*, vol. 2015-November, pp. 1261–1264, 2015.

[28] A. N. Skauen, "Ship tracking results from state-of-the-art space-based AIS receiver systems for maritime surveillance," *CEAS Space Journal*, vol. 11, no. 3, pp. 301–316, sep 2019.

[29] H. Sanchez, D. Mcintosh, H. Cannon, C. Pires, J. Sullivan, S. D'Amico, and B. O'connor, "Starling1: Swarm Technology Demonstration," in *32nd Annual AIAA/USU Conference on Small Satellites*, 2018.

[30] Sky and Space Global Ltd, "SAS '3 Diamonds' Nano-Satellites Generate First Revenues," Mar. 2018, accessed 14.11.2019. [Online]. Available: https://www.investi.com.au/api/announcements/sas/5422b146-a4c.pdf

[31] A. Klesh and J. Krajewski, "MarCO: CubeSats to Mars in 2016," in *29th Annual AIAA/USU Small Satellite Conference*, 2015.

[32] J. Esper, S. Neeck, J. A. Slavin, W. Wiscombe, and F. H. Bauer, "Nano/Micro Satellite Constellations for Earth and Space Science," *Acta Astronautica*, vol. 52, no. 9-12, pp. 785–791, may 2003.

[33] LACMA, "ENOCH," accessed 14.11.2019. [Online]. Available: https://www.lacma.org/lab/project/enoch

[34] G. Nies, M. Stenger, J. Krčál, H. Hermanns, M. Bisgaard, D. Gerhardt, B. Haverkort, M. Jongerden, K. G. Larsen, and E. R. Wognsen, "Mastering operational limitations of LEO satellites – The GomX-3 approach," *Acta Astronautica*, vol. 151, no. April, pp. 726–735, oct 2018.

[35] D. Gerhardt, M. Bisgaard, L. Alminde, R. Walker, M. A. Fernandez, A. Latiri, and J.-L. Issler, "GOMX-3: Mission Results from the Inaugural ESA In-Orbit Demonstration CubeSat," in *30th Annual AIAA/USU Conference on Small Satellites*, 2016.

[36] L. L. Pérez, P. Koch, and R. Walker, "GOMX-4 – the twin European mission for IOD purposes," in *32nd Annual AIAA/USU Conference on Small Satellites*, 2018.

[37] L. L. Pérez, P. Koch, D. Smith, and R. Walker, "GOMX-4, the most advance nanosatellite mission for IOD purposes," in *The 4S Symposium*, 2018.

[38] GomSpace A/S, "NanoPower BP4 Datasheet High Capacity battery pack for nano-satellites featuring four Li-Ion cells," 2018, accessed on 11.07.2019. [Online]. Available: https://gomspace.com/UserFiles/Subsystems/datasheet/gs-ds-nanopower-bp4-27.pdf

[39] ——, "NanoPower BPX Datasheet High-capacity battery pack for nano-satellites," 2018, accessed on 11.07.2019. [Online]. Available: https://gomspace.com/UserFiles/Subsystems/datasheet/gs-ds-nanopower-bpx-3-18.pdf

[40] ——, "NanoPower Battery Datasheet Lithium Ion 18650 cells for space flight products," 2018, accessed on 11.07.2019. [Online]. Available: https://gomspace.com/UserFiles/Subsystems/datasheet/gs-ds-nanopower-battery-17.pdf

[41] Y. Borthomieu, "Satellite Lithium-Ion Batteries," in *Lithium-Ion Batteries*. Elsevier, 2014, pp. 311–344.

[42] V. Knap and D.-I. Stroe, "Effects of open-circuit voltage tests and models on state-of-charge estimation for batteries in highly variable temperature environments: Study case nano-satellites," *Journal of Power Sources*, vol. 498, p. 229913, jun 2021.

Vaclav Knap received his M.Sc. from Aalborg University, Denmark in Electrical Power Systems and High Voltage Engineering, where he started to pursue research in field of Lithium-ion batteries, their lifetime modeling and utilization for grid applications. Vaclav received his Ph.D degree in topic "Advance management system for Lithium-Sulfur batteries" at the same university in 2017, where he tackled the challenges for the practical use of Lithium-Sulfur batteries in the practical applications. Since 2019, he works as an industrial postdoc across GomSpace, a CubeSat developing company, Aalborg University and Czech Technical University in Prague, where he is focusing on Lithium-ion battery management systems and battery lifetime in CubeSats.

Szymon Beczkowski received the M.Sc. degree in electrical engineering from the Warsaw University of Technology, Poland, in 2007. In 2012, he received the Ph.D. degree from Aalborg University, Aalborg, Denmark.

He is currently working as Associate Professor at the Department of Energy Technology, Aalborg University. His research interests include optimisation of power electronic converters, power module packaging and SiC technology.

Lars Kjeldgaard Vestergaard received his M.Sc. degree in control engineering from Aalborg University, Denmark, in 2006. He has been working in the electronics industry in Denmark in various companies, mostly with electronics design, and has been working at GomSpace A/S in Denmark since 2017. He is currently working as Technology Manager at GomSpace A/S, focusing on optimizing product assurance activities, including processes, and test and qualification of products.

Daniel-Ioan Stroe received the Dipl.-Ing. degree in automatics from "Transilvania" University of Brasov, Romania, in 2008, and M.Sc. degree in wind power systems from Aalborg University, Aalborg, Denmark, in 2010. He has been with AAU Energy, Aalborg University since 2010, from where he obtained his Ph.D. degree in lifetime modeling of Lithium-ion batteries in 2014. He is currently an Associate Professor with AAU Energy and the leader of the Batteries research group. He was a Visiting Researcher with RWTH Aachen, Germany, in 2013. He has co-authored over 150 scientific peer-review publications most of them on topics related to Lithium-ion battery performance and lifetime modeling and battery state estimation. Furthermore, he is serving as a special issue editor and topic editor for various journals. Daniel's current research interests are in the area of energy storage systems for grid and e-mobility, Lithium-based battery testing and modeling, and lifetime estimation and diagnostics of Lithium-ion batteries.